Materials Research. 2021; 24(4): e20200580
DOI: https://doi.org/10.1590/1980-5373-MR-2020-0580

Effect of Na_2WO_4 Concentration on the Microstructure and Corrosion Behavior of Ni-W-P Ternary Alloy Coatings

***Sha-sha Tian*[a], *Wan-chang Sun*[a]*, *Yu-wan Liu*[a], *Ya-peng Jia*[a], *Yan Xiao*[a]**

[a] *Xi'an University of Science and Technology, College of Materials Science and Engineering, Xi'an, Shaanxi 710054, P.R.China.*

Received: December 20, 2020; Revised: April 30, 2021; Accepted: May 18, 2021

Ni-W-P ternary coating was successfully deposited on AZ91D magnesium alloy by electroless plating with low energy consumption. The effect of Na_2WO_4 concentration on the microstructure, deposition rate, corrosion behavior, adhesion force, porosity test and micro-hardness of Ni-W-P ternary coatings were evaluated. Results reveal that when the concentration of Na_2WO_4 is 15 g/L in the plating solution, the coating with the average thickness of 17 μm is uniform and dense, and the content of phosphorus and tungsten reached 9.63 wt.% and 1.14 wt.% respectively, which presents amorphous structure. Meanwhile, when the concentration of Na_2WO_4 is 15 g/L, the amorphous Ni-W-P ternary coating has the best corrosion resistance, among which E_{corr} is -0.326 V, I_{corr} is 0.003 A/cm^2 in 3.5 wt.% NaCl solution. In addition, the mechanisms of corrosion resistance for the substrate and the coating were exploded.

Keywords: *Magnesium alloy, Ni-W-P ternary coating, Electroless, Microstructure, Corrosion behavior.*

1. Introduction

Magnesium and magnesium alloys, due to their excellent properties such as low density, high strength and stiffness and electromagnetic shielding, have been widely used in various industries such as aerospace, automobile, medical treatment and electronics[1-4]. Regrettably, the poor corrosion resistance, wear resistance, creep resistance and high chemical activity in aggressive environment limits the magnesium alloy in practical application[5,6]. Thereby, improving the performance of magnesium alloys is a hot research topic at present[7,8].

The poor corrosion resistance of magnesium alloy is a problem that needs to be solved in time. For this purpose, the effective way of preventing corrosion is through the formation of a protective coating which acts as the barrier between the corrosive medium and the substrate[9-11]. Among various surface treatments[12,13], environmentally friendly electroless plating without external power is advantageous to form a uniform and crack-free coating[14-18]. Therefore, electroless may be a promising candidate to face with the inevitable problems and extend the use of magnesium alloys[19,20].

Electroless Ni-P binary alloy coatings have unique physical and chemical properties and have been widely used in industry[21,22]. As we all known, the P content largely determines the properties of Ni-P coatings[23]. Because amorphous state without grain boundaries prevents corrosive media to diffuse, the amorphous structure Ni-P coatings with high content P act as a protective role in corrosive media[19]. Nevertheless, with the development of industrial production, the requirements for materials in terms of corrosion resistance, wear resistance, magnetic properties, and hardness are higher[24,25], but binary Ni-P alloy coatings often cannot meet the requirements[26,27]. Electroless Ni-based ternary coating has better properties than electroless Ni-P coating in all aspects, such as thermal stability, wear resistance, corrosion resistance and so on. It shows a very considerable application prospect in engineering application[28].

It is well-known that tungsten can easily be included in electroless Ni-P coatings and has good corrosion resistance[29,30]. At the same time, the amorphous Ni-W-P coating has high resistivity and low resistance temperature coefficient, which can be used as the protective layer of medical devices and other parts. Shao et al.[31] confirmed that the Ni-W-P coating can be applied for corrosion protection in salty environment and exhibited superior corrosion resistance. Owning to the Ni-W-P coating has so many excellent properties and is widely used, a growing number of people research it. Shu et al.[32] researched coating mechanical properties including hardness and wear resistance. Biswas et al.[33] analyzed the effect of various heat treatment conditions on the phase transformation behavior of electroless Ni-P-W coating and tried to link them with the tribological characteristics of the coating hardness, friction, wear and scratch hardness.

Herein, the synthesis of a novel and robust anti-corrosion Ni-W-P ternary amorphous coating on AZ91D magnesium alloy substrates was achieved by electroless. The microstructure, deposition rate, corrosion behavior, bond strength, porosity test and micro-hardness of Ni-W-P ternary coatings containing various Na_2WO_4 concentrations were comparatively investigated. The corrosion mechanism of magnesium alloy and the corrosion resistance mechanism of coating were discussed.

*e-mail: sunwanchang@tsinghua.org.cn

2. Experimental Methods

2.1. Pretreatments

AZ91D magnesium alloy substrates with a size of 15 mm×10 mm×20 mm were polished initially with abrasive paper of 150, 600, 800, 1200, 1500 grit by sequence to remove impurities. The substrates were washed by ultrasonic vibration in acetone for 10 min, and subsequently eliminated via a 15 min process employing alkaline solution. Subsequently, the samples were immersed in zinc dipping solution to obtain zinc layer with the purpose of improving the adhesion between the magnesium alloy substrate and the copper layer and preventing the magnesium alloy substrate from corrosion in the copper plating solution. In the end, the surface of the magnesium alloys was plated with copper as undercoat layer by electroless, which can improve the adhesion between the substrate and the Ni-W-P coatings[34]. The formulas and operating conditions of zinc dipping and copper preplating are shown in Table 1 and Table 2 respectively.

2.2. Electroless of the Ni-W-P coatings

The reasonable composition of the plating solution is the basis for the preparation of high quality electroless nickel alloy. And the main components of the plating solution in this experiment are: main salt $NiSO_4 \cdot 6H_2O$, reducing agent, complexing agent, accelerator and stabilizer. The specific formula of plating solution and operating conditions of Ni-W-P coatings is shown in Table 3.

2.3. Characterization

The surface morphologies of Ni-W-P coatings were analyzed by scanning electron microscope (SEM, JSM-6390A, Japan). The composition of the coatings was analyzed using the energy dispersive spectroscopy (EDS) spectrometer provided with the SEM. And the phase composition of the Ni-W-P coating was determined by X-ray diffractometer (XRD-7000, Shimadzu, Japan). The Cu-Kα target was used, with a scanning speed of 8 °/s and a scanning range of 10°-80°.

2.4. Electrochemical measurements

The polarization curves of the samples were measured by three electrode system in 3.5 wt.% NaCl solution. The paraffin sealed sample (10 mm×10 mm in area) was used as the working electrode, the saturated calomel electrode was put into the salt bridge as the reference electrode, and the platinum sheet as the auxiliary electrode. 3.5wt % NaCl solution was the corrosion electrolyte.

PGSTAT302N electrochemical workstation produced by Swiss Wantong company was used. The samples were immersed in the corrosive solution for 30 min before the EIS tests to establish the steady state condition. The scanning rate of polarization curve was 1 mV/s and the scanning range of potential was -1.8 V~0 V. Impedance spectrum is an electrical measurement method with small amplitude sine wave potential as disturbance signal. The parameters of EIS were as follows: amplitude is 10 mV, frequency scanning range is 10 kHz~0.01 Hz at open circuit potential (OCP) with 20 mV sinusoidal perturbation.

The corrosion rate of the Ni-W-P coating was measured by total immersion corrosion test. The weight loss method was used to calculate the corrosion rate. The calculation formula is shown in Equation 1. The corrosion rate was characterized by the change of coating mass per unit time and unit area.

$$V = \frac{m_1 - m_0}{S_0 \times t} \quad (1)$$

Where V is Corrosion rate (g/m² × h), m_1 is mass of the sample after corrosion (g), m_0 is mass of sample before corrosion (g), S_0 is immersing surface area (m²) and t is immersing time (h).

Table 1. The formulation and process of zinc immersion reaction.

Composition and operating parameters	Values
$ZnSO_4 \cdot 7H_2O$	60 g/L
Na_2CO_3	140 g/L
KF	3 g/L
PH	9~9.5
Temperature	71°C
Plating time	17 min
Stirring rate	100 r/min
Bath volume	0.5 L

Table 2. The formulation and process for the preparation of copper layer.

Composition and operating parameters	Values
$CuSO_4 \cdot 5H_2O$	50 g/L
$KNaC_4H_4O_6 \cdot 4H_2O$	140 g/L
NaOH	40 g/L
PH	11
Temperature	Room temperature
Plating time	1 h
Stirring rate	100 r/min
Bath volume	0.5 L

Table 3. Electroless bath composition and operating conditions of Ni-W-P coatings.

Composition and operating parameters	Values
$NiSO_4 \cdot 6H_2O$	30 g/L
Na_2WO_4	5~20 g/L
NaH_2PO_2	50 g/L
$Na_3C_6H_5O_7 \cdot 2H_2O$	25 g/L
NH_4F	10 g/L
CN_2H_4S	0.5~1 mg/L
PH	7~7.4
Temperature	60°C
Plating time	1 h
Stirring rate	300 r/min
Bath volume	0.5 L

2.5. Adhesion test

Adhesion test between Ni-W-P coatings and Mg alloy substrates were measured using a scratch test (WS-2005). The scratch speed was 5 mm/min, the loading rate was 50 N/min, and the scratch length was 4 mm. When the acoustic emission intensity is abrupt, the corresponding load is recorded as the critical load.

2.6. Porosity test

The Ni-W-P coatings on magnesium alloy must be pore-free, so we use the filter paper method to test the porosity of the coating[35]. The basic principle of filter paper method is to use a special reagent solution to contact the surface of the coating. The reagent solution reacts with the underlying metal or base metal through the pores of the coating to produce colored products. The porosity of the coating can be determined according to the number of spots. Reagent solution: 10 g/L NaCl, 106 g/L ethanol and 0.1 g/L phenolphthalein dissolved in deionized water. Then the filter paper with the reagent solution was pasted onto the samples for 10 min. After taking the filter paper away, red spots or red areas were noted on the surface of the coating. The porosity of coating is evaluated relatively by the ratio of red spot area to the zone area previously pasted by the filter paper[36].

2.7. Vickers micro-hardness

The micro-hardness of the Ni-W-P coatings was tested using an HV-1000 type hardness tester with a load of 200 gf and duration of 10 s. Three tests were performed for each coated sample and the results were averaged.

3. Results and Discussion

3.1. Microstructures and composition of Ni-W-P coating

The surface morphologies of the Ni-W-P coatings deposited by electroless with different Na_2WO_4 concentrations are indicated in Figure 1a-d. As can be seen from Figure 1a-d that the surface morphologies of Ni-W-P coatings present cellular protrusion, and the coatings are relatively flat without obvious defects such as pores, cracks and holes. However, by comparing Figure 1c with Figure 1a, b, d, we can see that the surface morphology of the Ni-W-P coating is more uniform and denser in Figure 1c in which the concentration of Na_2WO_4 is 15 g/L.

Figure 2a-d shows the cross-sectional morphologies of the Ni-W-P coating with different concentrations of Na_2WO_4, which are 5 g/L, 10 g/L, 15 g/L and 20 g/L, respectively. It can be found that from the cross-section morphologies presented in Figure 2a-d that the grey area on the left is magnesium alloy substrate, the dark grey part on the right is the Ni-W-P coatings, and in the middle is a thin copper layer. When the concentration of Na_2WO_4 is 15 g/L, the thickness of the coating is the largest, reaching 17 μm. The Ni-W-P coatings have good adhesion with the magnesium alloy substrate, and the coatings are uniform without obvious cracks, voids and other defects from Figure 2. Compared with Figure 2c and Figure 2a, b, d, the interface between the Ni-W-P coating and the resin is flatter, and it is further verified that the surface morphology of the Ni-W-P coating with 15 g/L Na_2WO_4 is more compact. In theory, there is a zinc layer formed in the process of zinc dipping between magnesium alloy substrate and copper layer. However, the zinc layer is too thin to be observed clearly. At the same time, the interface is clear and smooth.

Known from EDS analysis of Ni-W-P coatings with different Na_2WO_4 concentrations presented in Figure 3a-d. Samples No. 1 to 4 represent Ni-W-P coatings with 5 g/L, 10 g/L, 15 g/L, and 20 g/L Na_2WO_4 in the plating solution respectively. The EDS shows that the Ni-W-P coatings consist of Ni, P and W. The mass percentages of elements in Ni-W-P coating are listed in Table 4. It can be observed from Table 4 that with the increase of Na_2WO_4 concentration in the plating solution, the mass percentage of P in No. 1 to No. 4 samples decrease from 9.89% to 7.90%, while the mass

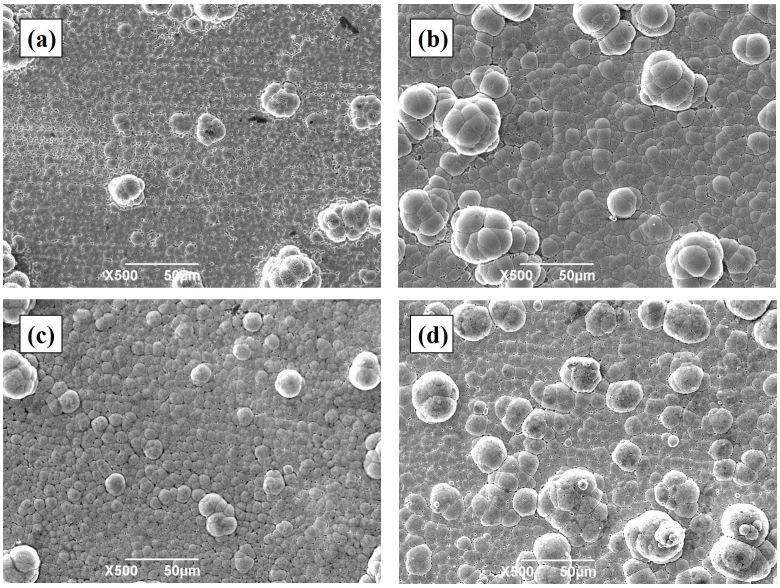

Figure 1. The surface morphologies of Ni-W-P coatings with different Na_2WO_4 concentrations. (a) 5 g/L (b) 10 g/L (c) 15 g/L (d) 20 g/L.

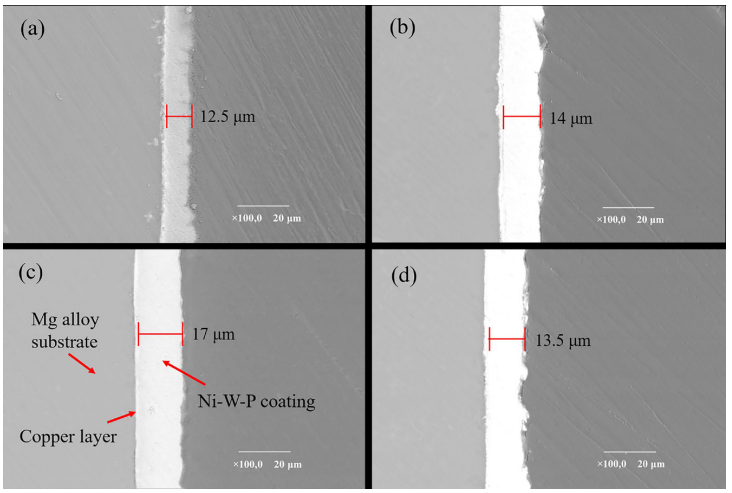

Figure 2. The cross-sectional morphologies of Ni-W-P coating with different Na_2WO_4 concentrations. (a) 5 g/L (b) 10 g/L (c) 15 g/L (d) 20 g/L.

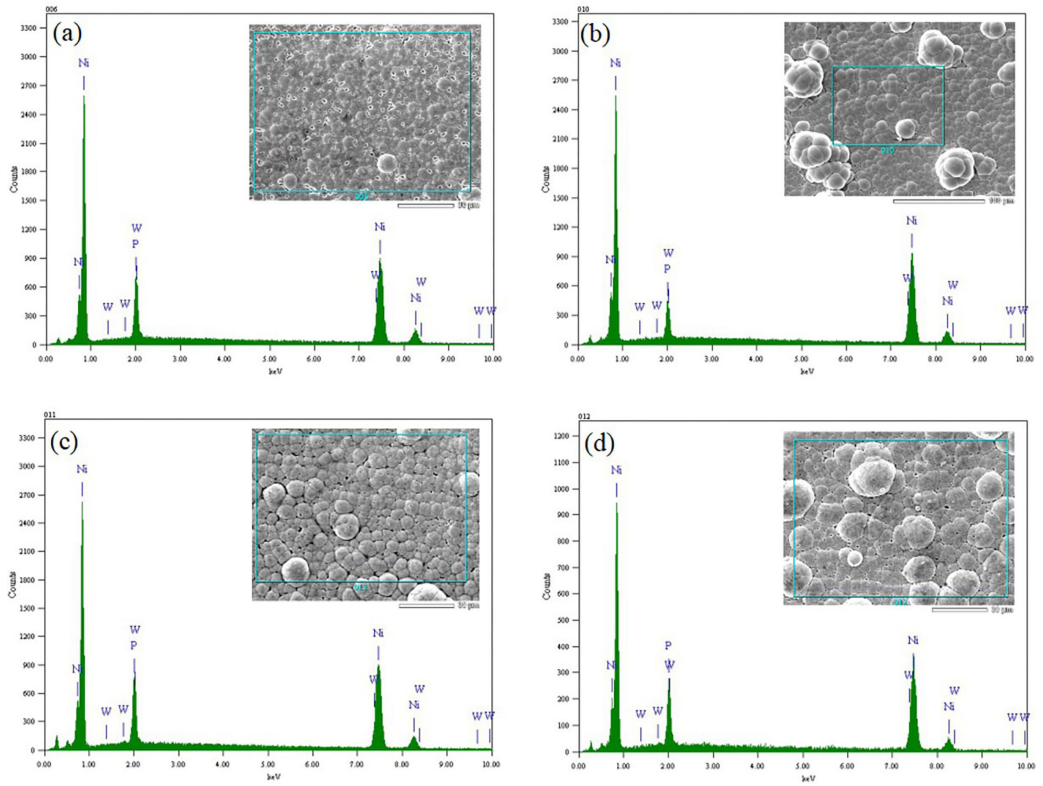

Figure 3. EDS of Ni-W-P coatings with different Na_2WO_4 concentrations. (a) 5 g/L (b) 10 g/L (c) 15 g/L (d) 20 g/L.

percentage of W increase from 0.61% to 1.24%. The results show that the addition of W has a certain blocking effect on the deposition reaction of P, thus reducing the mass fraction of P in the Ni-W-P coatings.

In addition, the mass fractions of P in the coatings of samples No. 1 to 3 all exceed 9%, Ni-W-P coatings have an amorphous structure. The mass fraction of P in sample No. 4 is 7.9% less than 9%, so the Ni-W-P coatings have a microcrystalline structure. In the process of deposition, with the increase of P content, the disorder degree of the Ni-W-P coating becomes larger and the amorphous structure is present. That is, with the increasing concentration of Na_2WO_4 in the plating solution, the Ni-W-P coatings evolve from an amorphous structure to a microcrystalline structure.

3.2. Effect of Na_2WO_4 concentration on deposition rate and phase composition of Ni-W-P coatings

The effect of the concentration of Na_2WO_4 in the plating solution on the deposition rate of the coatings is presented in Figure 4, which can be seen that the deposition rate of Ni-W-P coatings is accelerated with the increase of

Na_2WO_4 concentration in the plating solution. When the concentration of Na_2WO_4 is 15 g/L, the deposition rate of Ni-W-P coating is the fastest, about 17 μm/h. When the concentration of Na_2WO_4 exceeds 15 g/L, the deposition rate of Ni-W-P coating decreases rapidly. The reason for the accelerated deposition rate of Ni-W-P coatings may be that WO_4^{2-} may promote the co-deposition reaction. When the concentration of Na_2WO_4 in the plating solution exceed 15 g/L, the reason for the decrease of deposition rate is that the concentration of each component in the plating solution gradually decreases due to the continuous consumption of deposition reaction, resulting in the loss of the original proportion of each component content, thus reducing the deposition rate.

Figure 5 indicates the XRD spectra of the Ni-W-P coatings. Samples No.1 to 4 represent Ni-W-P coatings with 5 g/L, 10 g/L, 15 g/L, and 20 g/L Na_2WO_4 in the plating solution respectively. It can be seen from Figure 5 that the peaks corresponding to samples No.1, No.2 and No.3 are Ni (111) when the diffraction angle is $2\theta=45°$, which is a broad hump. Therefore, it can be inferred that the Ni-W-P coatings present an amorphous structure when the concentration of Na_2WO_4 is 5 g/L, 10 g/L and 15 g/L. Moreover, the peak of sample No.3 is lower than that of sample No.1 and sample No.2, which indicates that sample 3 has the highest degree of amorphization. According to the XRD spectra, the sharper the diffraction peak appears, the smaller the half-width of diffraction peak is, indicating that the crystallinity is better. Large half-width and low peak intensity show that the coating is microcrystalline or amorphous. The mass percentage of W in the Ni-W-P coatings of sample No. 4 increases and the mass percentage of P decreases to 7.90%, which eventually leads to the decrease of the driving force of the amorphous Ni-W-P coatings. However, the diffraction peaks of sample No. 4 are Ni (111) peak and Ni (220) peak, both of which are weak peaks and have a certain half-height width, indicating that the Ni-W-P coating has an amorphous structure. The result means that the Ni-W-P coating of sample No. 4 presents a microcrystalline structure mixed with amorphous structure and crystalline structure. This is consistent with the results of the energy spectrum analysis shown in Figure 3 and Table 4 above.

3.3. Corrosion resistance mechanism of Ni-W-P coating

Mg is relatively active and can easily form an oxidation film in the air. and its structure was shown in Figure 6. This oxide film consists of three layers. The outer layer is lamellar, the middle layer is the densest oxide layer, and the inner layer is porous. The oxide film of this structure is brittle and porous, which is easy to be corroded, and has no protective effect on magnesium alloy substrate.

Unstable passivated magnesium hydroxide films formed on the surface of magnesium can be destroyed in the presence of Cl^-, $SO_4^{2-}$and NO_3^- plasma or exposed to water containing acidic gases (such as CO_2). Therefore, they cannot provide long-term protection for the matrix alloy, resulting in pitting corrosion. Due to the addition of solute element W with self-passivation property, the grain size of the coating is refined, and more W is diffused to the surface by the

Table 4. The results of energy spectrum analysis of Ni-W-P coatings.

Sample	Ni (wt.%)	P (wt.%)	W (wt.%)
No. 1	89.50	9.89	0.61
No. 2	89.34	9.81	0.85
No. 3	89.23	9.63	1.14
No. 4	90.86	7.90	1.24

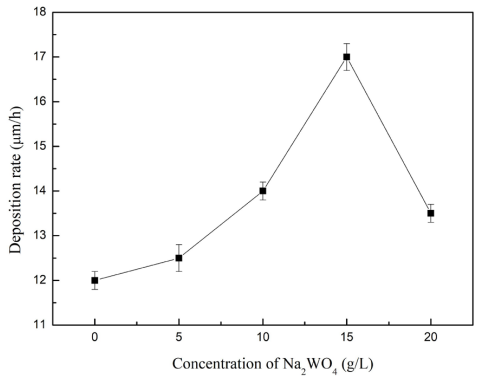

Figure 4. Effect of the concentration of Na_2WO_4 in plating solution on deposition rate.

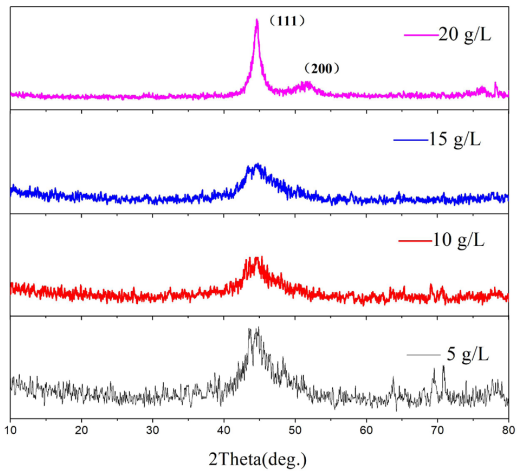

Figure 5. XRD spectra of Ni-W-P coatings with different Na_2WO_4 concentrations in plating solution.

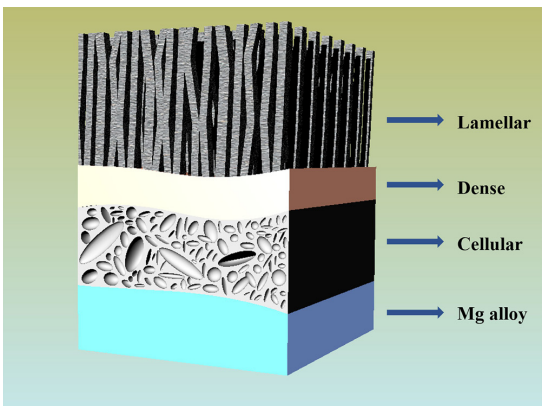

Figure 6. Schematic of oxide film for corrosion of magnesium alloy in air environment.

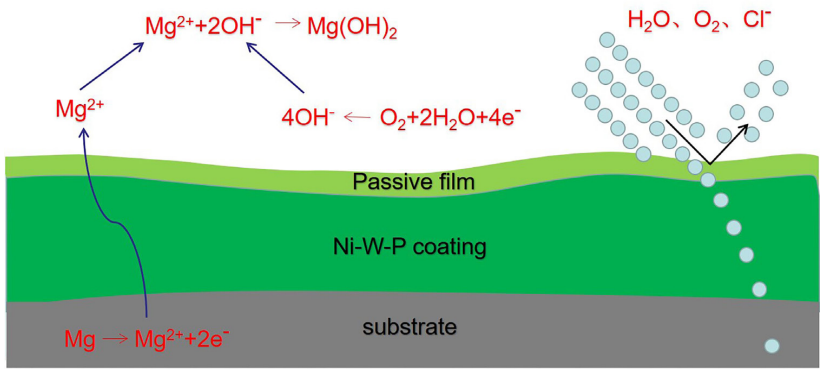

Figure 7. Anti-corrosion mechanism for Ni-W-P coating.

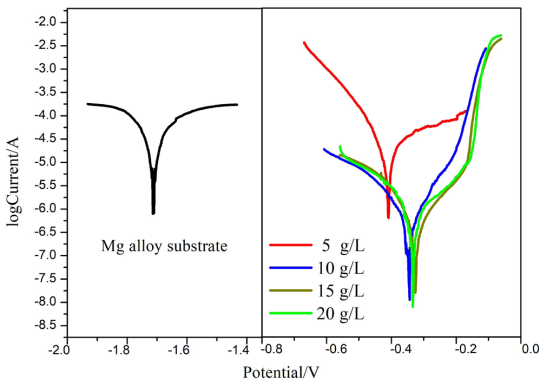

Figure 8. Polarization curves of magnesium alloy and Ni-W-P coatings with different Na_2WO_4 concentrations in 3.5 wt.% NaCl solution.

Table 5. Fitting parameters for the polarization curves of magnesium alloy and Ni-W-P coatings in 3.5 wt.% NaCl solution.

Sample	Na_2WO_4 concentration (g/L)	E_{corr}(V)	I_{corr}(A/cm^2)
Ma alloy substrate	0	-1.710	23.188
No. 1	5	-0.410	0.254
No. 2	10	-0.344	0.012
No. 3	15	-0.326	0.003
No. 4	20	-0.334	0.057

diffusion channel, thus forming a complete passive film on the surface. Based on the advantages of Ni-W-P coating in the field of corrosion protection, it can well block water molecules, oxygen molecules and other ions in the air, thus protecting the magnesium alloy substrate. The anti-corrosion mechanism of Ni-W-P coating is shown in Figure 7.

3.4. Effect of Na_2WO_4 concentration on corrosion resistance of Ni-W-P coatings

The electroless Ni-W-P coatings are designed to improve the corrosion resistance of the magnesium alloy substrate to protect it. The polarization curves of magnesium alloy substrate and Ni-W-P coatings in 3.5 wt.% NaCl solution are shown in Figure 8. Table 5 shows the fitting results of the polarization curves of the magnesium alloy substrate and the Ni-W-P coatings. As can be seen from Table 5, the self-corrosion potential of the magnesium alloy substrate is about -1.71 V, and the corrosion current is 23.188 A/cm^2. According to Figure 8 and Table 5, the corrosion current of sample No. 1 is 0.254 A/cm^2 and the self-corrosion potential is -0.41 V, which much higher than that of the magnesium alloy substrate (-1.710 V). The corrosion current is significantly lower than that of the magnesium alloy substrate (23.188 A/cm^2). It shows that the corrosion rate of the coatings of sample No. 1 is slow and it is not easy to be corroded.

The corrosion potential of sample No.3 is -0.326 V, and its corrosion current is 0.003 A/cm^2. The results show that the mass fraction of W in the coatings of No.3 increases, while the mass fraction of P only decreases slightly. Therefore, the self-corrosion potential of the No.3 is shifted forward compared with that of the sample No.1 and No.2, and the corrosion current of No.3 is decreased. In summary, the Ni-W-P amorphous coatings of sample No.3 with 15 g/L Na_2WO_4 added has the optimal corrosion resistance and can well protect the magnesium alloy substrate from corrosion.

Figure 9 shows the impedance spectra of Ni-W-P coatings in 3.5 wt.% NaCl solution (Figure 9a) and the corresponding bode spectra (Figure 9b, c). The Nyquist diagram is drawn with the imaginary impedance value as a function of the real part. In the impedance spectrum in Figure 9a, only one capacitive reactance arc appears. The impedance spectrum in Figure 9a only shows a capacitive reactance arc. Generally, the polarization resistance of the sample is negatively correlated with the corrosion rate. The polarization resistance is represented by the impedance semicircle radius. When the radius is larger, the polarization resistance is higher; the corrosion rate is smaller, so the corrosion resistance is better. As can be seen from Figure 9a, the corrosion resistance of sample No. 1 is the weakest. With the increase of the amount of Na_2WO_4 in the plating solution, the corrosion resistance of samples No. 1 to No. 3 gradually increases, while the corrosion resistance of sample No. 4 decreases compared to that of No. 3. The above results are related to the degree of amorphization of the Ni-W-P coatings. The corrosion resistance of the amorphous coatings is stronger than that of the microcrystalline and crystalline coatings. Because the Ni-W-P coating of sample No. 4 shows a microcrystalline structure, its corrosion resistance is not as good as that of No. 3.

The Bode1 diagram (Figure 9b) is drawn based on the impedance modulus |Z| as a function of frequency. The Bode

Table 6. Electrochemical parameters from EIS data of magnesium alloy and Ni-W-P coatings with different Na_2WO_4 concentrations in 3.5 wt.% NaCl solution.

Sample	Na_2WO_4 concentration (g/L)	$R_s(\Omega \cdot cm^2)$	$Y_{0,dl}(S^n \cdot \Omega^{-1} \cdot cm^{-2})$	n	$R_{ct}(\Omega \cdot cm^2)$	$\chi^2/10^{-3}$
Ma alloy substrate	0	16.62	2.54×10^{-5}	0.82	3.76×10^{2}	1.3
No. 1	5	12.25	1.83×10^{-5}	0.93	1.24×10^{4}	3.6
No. 2	10	12.21	1.41×10^{-5}	0.93	2.72×10^{4}	2.3
No. 3	15	11.87	1.27×10^{-5}	0.92	3.51×10^{4}	4.1
No. 4	20	11.93	2.48×10^{-5}	0.85	2.03×10^{4}	3.2

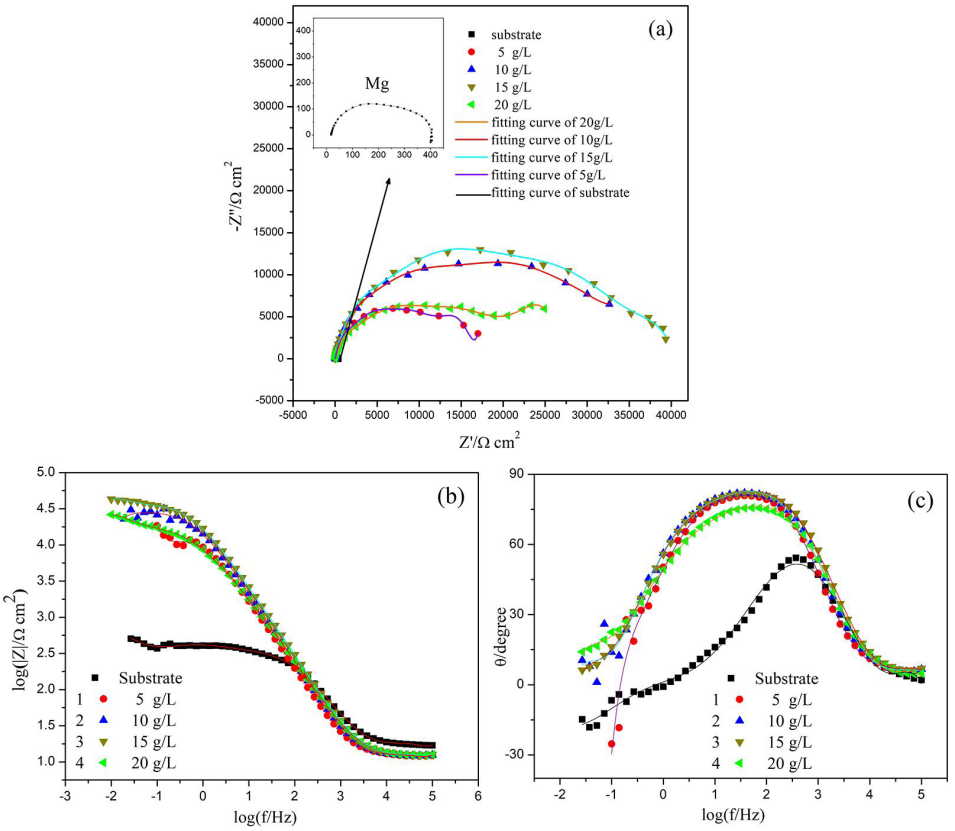

Figure 9. The impedance spectra of magnesium alloy and Ni-W-P coatings in 3.5 wt.% NaCl solution.

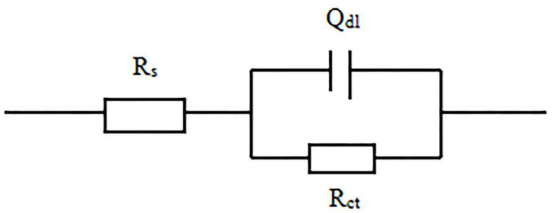

Figure 10. Equivalent Circuit for the impedance spectra.

2 diagram (Figure 9c) shows that the Ni-W-P coatings have a single time constant in the NaCl solution. The results show that the coating containing W can prevent the contact between corrosion solution and magnesium alloy substrate, and has excellent corrosion resistance. However, in the Bode1 diagram, the |Z| of the coatings of sample No. 1 is the smallest. With the increase concentration of Na_2WO_4 in the plating solution, the |Z| value of sample No. 4 decreases instead. The results indicate that the Ni-W-P coating containing 15 g/L Na_2WO_4 has the best corrosion resistance of sample No. 3, which is consistent with the polarization curve.

Figure 10 is the equivalent circuit diagram fitted by the Nyquist diagram of Ni-W-P coatings. In the fitting circuit, R_s is the resistance of the electrolyte solution, Q_{dl} represents the constant phase angle component of the electric double layer capacitor, and R_{ct} is the charge transfer resistance, which controls the circuit. The data after fitting the equivalent circuit diagram is listed in Table 6. According to the fitted data, the concentration of Na_2WO_4 added in the plating solution has a greater impact on the charge transfer resistance Rct. The charge transfer resistance Rct of samples No. 1 to No. 4 is significantly larger than that of the magnesium alloy substrate ($3.76\times10^2\ \Omega \cdot cm^2$). It observes that the Ni-W-P coatings with different Na_2WO_4 concentrations in the plating solution can greatly improve the corrosion resistance of the magnesium alloy substrate. Table 6 shows that with the increase of Na_2WO_4 concentration in the plating solution, the Rct of samples No. 1 to No. 3 increase from $1.24\times10^4\ \Omega \cdot cm^2$ to

3.51×10^4 Ω·cm^2. Sample No. 3, the Ni-W-P coatings with 15 g/L of Na_2WO_4 added in the plating solution, has the largest charge transfer resistance Rct, but Rct of sample No. 4 is reduced to 2.03×10^4 Ω·cm^2.

The above fitting results illustrate that with the increase of Na_2WO_4 concentration in the plating solution, the corrosion resistance of Ni-W-P coatings gradually raises. When the concentration of Na_2WO_4 is 15 g/L, the R_{ct} of Ni-W-P coatings is the largest, and the corrosion performance is the best. Whereas the concentration of Na_2WO_4 exceeds 15 g/L, the corrosion resistance of the Ni-W-P coatings will decline instead. The conclusion is consistent with the result drawn by the above polarization curve and Nyquist diagram.

The corrosion rates measured for the Ni-W-P coatings after immersion in 3.5 wt.% NaCl solution for 72 h are shown in Figure 11. It can be observed that the corrosion rate of sample No. 1 is the fastest, about 0.6146 g/m^2·h, that of sample No. 2 is 0.1076 g/m^2·h, and that of sample No. 3 is 0.0903 g/m^2·h. The corrosion rates of sample No. 2 and No. 3 are obviously lower than those of No. 1. It shows that the increase of Na_2WO_4 concentration in the plating solution, the corrosion rates of the coatings gradually decrease, and the corrosion resistance gradually improves. However, the corrosion rate of sample No. 4 (0.4401 g/m^2·h) is accelerated, indicating that its corrosion resistance is not as good as that of samples No. 2 and No. 3.

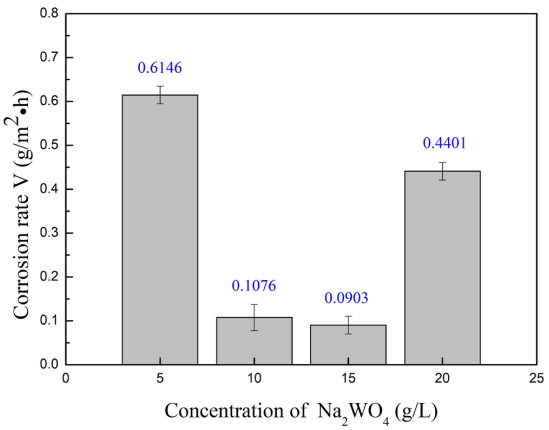

Figure 11. Corrosion rate of Ni-W-P coatings with different concentrations of Na_2WO_4 in 3.5 wt.% NaCl solution for 72 h.

The above results show that the corrosion rates of Ni-W-P coatings decrease with the rise of Na_2WO_4 concentration from 5 g/L to 15 g/L, and the corrosion resistance increases gradually. However, the corrosion rate (0.4401 g/m^2·h) of sample No.4 with 20 g/L Na_2WO_4 in the plating solution is faster than that of No.2 and No.3. The result is consistent with the above polarization curve (Figure 8) and impedance spectrum analysis (Figure 9).

Figure 12 reveals the corrosion morphologies of the Ni-W-P coatings after immersion in 3.5 wt.% NaCl solution for 72 h. From Figure 12a which shows the corrosion morphology of No. 1, we can see that there is a high degree of corrosion, and there are serious corrosion pits, so the surface morphology of the coating cannot be identified. The sample No. 3 (Figure 12c) has a relatively low degree of corrosion, with a few corrosion pits on the surface, and the cellular surface morphology is clearly visible. In addition, the corrosion degree of sample No. 4 (Figure 12d) is heavier than that of Figure 12c, and the phenomenon of coating peeling occurs. Therefore, we can conclude that with the increase concentration of Na_2WO_4, the corrosion resistance of the Ni-W-P coatings is gradually improved, so the sample No. 3 has the best corrosion resistance. On the contrary, the excessive concentration of Na_2WO_4 in the plating solution will reduce the corrosion resistance of the Ni-W-P coatings.

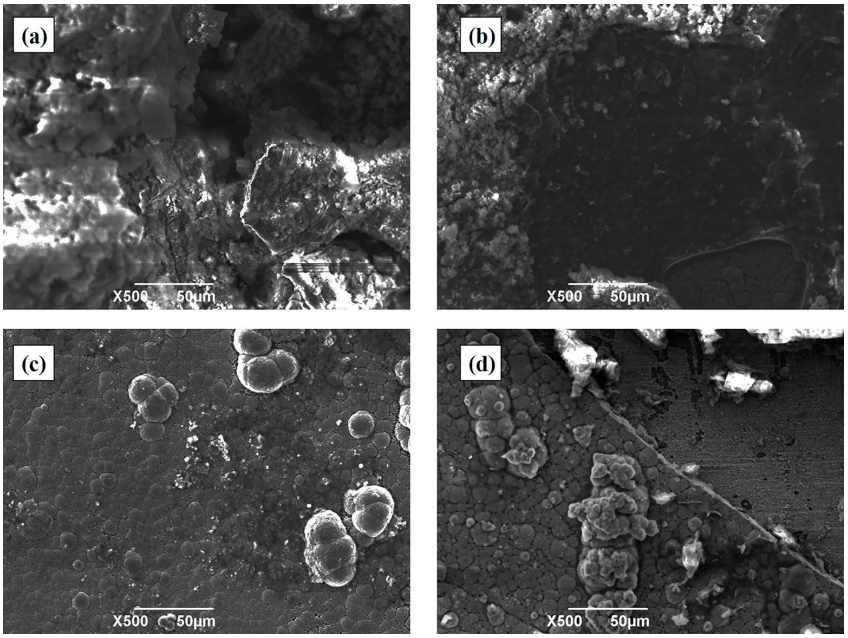

Figure 12. Corrosion morphologies of Ni-W-P coatings with different Na_2WO_4 concentrations immersed in 3.5 wt.% NaCl solution for 72 h. (a) 5 g/L (b) 10 g/L (c) 15 g/L (d) 20 g/L.

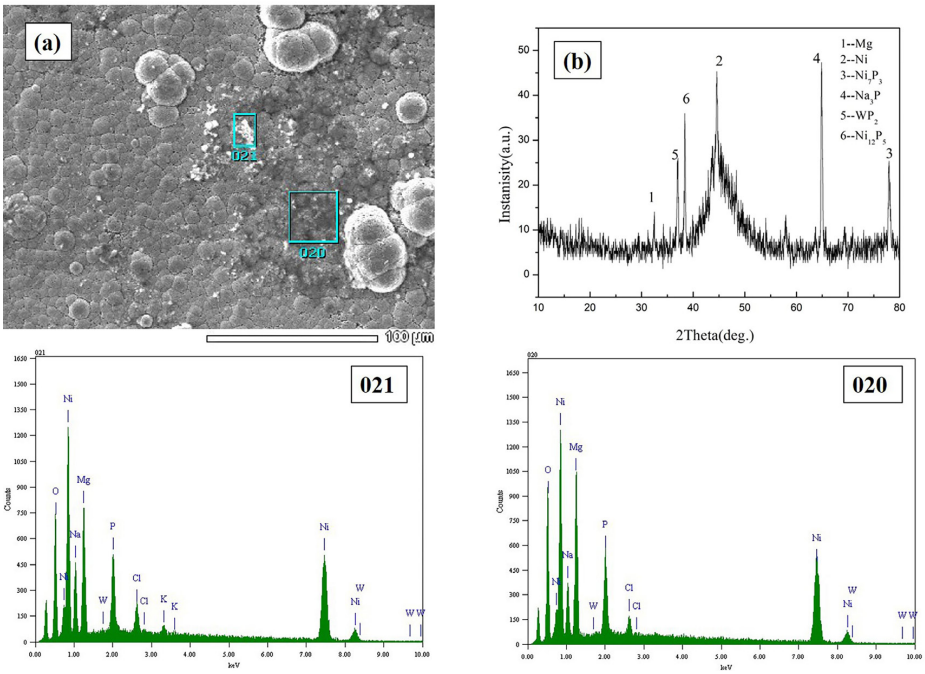

Figure 13. (a) Energy spectrum analysis of Ni-W-P coatings immersed in 3.5 wt.% NaCl solution for 72 h. (b) XRD diffraction of Ni-W-P coatings immersed in 3.5 wt.% NaCl solution for 72 h.

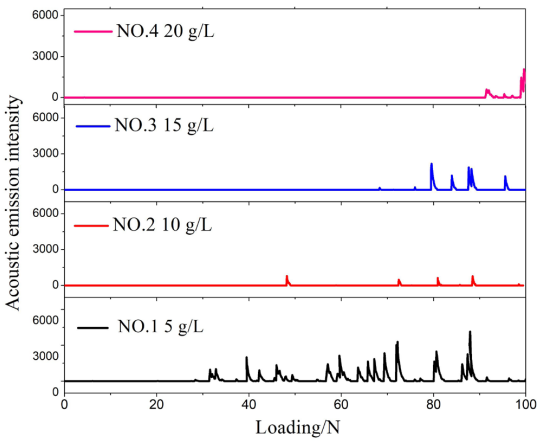

Figure 14. Scratch curves of Ni-W-P coatings.

Because the amorphous structure has fewer defects in grain boundaries and dislocations, its corrosion resistance is better than that of microcrystalline structures. From the analysis of the XRD phase composition in Figure 5, the samples No. 1 to No. 3 all have amorphous structure, while the sample No. 4 shows crystalline structure. In addition, due to the supplement of W, the porosity of the coatings is reduced, and a passivation film is easily formed in the atmosphere, acidic or alkaline corrosive media. When corrosion occurs, Ni-W-P coating will be activated and dissolved rapidly, promoting the accumulation of passivation elements to the surface, which provides conditions for the formation of a good passive film. When the passive film is damaged, it can repair itself quickly, so the Ni-W-P coatings have excellent corrosion resistance.

However, if the mass fraction of W in Ni-W-P coatings is too high, the mass fraction of P will be reduced and the phase composition of Ni-W-P coating will be changed. Under the same conditions, the corrosion resistance of microcrystalline structure is not as good as that of amorphous structure. Therefore, the Ni-W-P ternary amorphous coatings of 15 g/L Na_2WO_4 have the best corrosion resistance.

Figure 13 shows the EDS and XRD pattern of Ni-W-P coatings with 15 g/L Na_2WO_4 added to the plating solution. From the EDS analysis (Figure 13a), elements such as Mg, Ni, P, and W exist on the corrosion surface of the Ni-W-P coatings. From the analysis of XRD pattern in Figure 13b, the corrosion peak of Ni-W-P coatings shows Mg, which indicates that the surface of Ni-W-P coatings are partially exfoliated and the magnesium alloy substrate is exposed. Similarly, the XRD reveals that the products after corrosion are mainly Ni-P compounds, WP_2, Na_3P, etc. There are still scattered diffraction peaks in the XRD pattern, indicating that the amorphous structure of the Ni-W-P coatings in some regions have not changed during immersion. The above shows that the presence of Ni-W-P coatings can slow down the corrosion of magnesium alloy and improve the corrosion resistance of magnesium alloy.

3.5. Adhesion between Ni-W-P coatings and Mg alloy substrates

Figure 14 is the scratch curves between acoustic emission signal of Ni-W-P coating surface and pressure loading (K-L). According to Figure 14, the critical load of sample NO. 1 is 31.55 N, that of NO. 2 is 48.2 N, that of NO. 3 is 79.45 N, and that of NO. 4 is 91.4 N. As can be seen from the above, with the increase of Na_2WO_4 concentration in the plating solution, the critical load Lc value of Ni-W-P coatings

Table 7. The Vickers micro-hardness of Ni-W-P coatings with different Na_2WO_4 concentrations.

Sample	Test 1, HV	Test 2, HV	Test 3, HV	Average HV/MPa
No. 1(5 g/L)	186.2	130.8	116.2	144.4
No. 2(10 g/L)	157.0	137.2	143.3	145.8
No. 3(15 g/L)	269	267.3	270.9	269.1
No. 4(20 g/L)	359.4	373.8	311.6	348.3

arguments step wisely, and the adhesion strength increases gradually. At the same time, the Ni-W-P coatings, with the concentration of Na_2WO_4 is 20 g/L, have the best bonding strength and the best adhesion. Apparently,the addition of W in the coatings can effectively reduce and hinder the formation of cracks, thereby improving the bonding force between the Ni-W-P coatings and the magnesium alloy substrate.

3.6. Effect of Na_2WO_4 concentration on porosity of Ni-W-P coatings

The surface of Ni-W-P coatings with different concentrations of sodium tungstate was observed by visual inspection porosity test in all cases. The observations depicted that there is no red spot on the surface of the pasted filter papers. When the concentration of Na_2WO_4 is 5 g/L and 10 g/L, only one and three red spots appear on the filter paper. When the concentration of Na_2WO_4 is 15 g/L and 20 g/L, there is no red spot, which indicates that the Ni-W-P coating is completely pore-free and plays a role in protecting the magnesium alloy substrate.

The results of the porosity tests show that the structure of the electroless Ni-W-P coatings is compact enough which impedes the diffusion of the porosity test solution after about 10 min contact time between the soaked filter paper and the surface of the coated samples. At the same time, it is verified that the surface of the Ni-W-P coatings is more uniform and compact when the concentration of Na_2WO_4 is 15 g/L.

3.7. Effect of Na_2WO_4 concentration on micro-hardness of Ni-W-P coatings

Table 7 shows the Vickers micro-hardness of Ni-W-P coatings with different Na_2WO_4 concentrations. Each sample is tested three times and the average value is obtained by calculation. It can be seen from Table 7 that with the increase of Na_2WO_4 concentrations, the micro-hardness of the Ni-W-P coatings increases gradually. When the concentration of Na_2WO_4 is 15 g/L and 20 g/L, the Vickers micro-hardness of the coating reaches 269.1 MPa and 348.3 MPa. This may be due to the addition of solute element W with self-passivation characteristics, which makes the coating finer grain size, more compact grain boundaries, and homogeneous crystalline structure.

4. Conclusions

(1) Ni-W-P ternary coatings were successfully deposited on the surface of AZ91D magnesium alloy substrates by proposed method of electroless. Ni-W-P coatings had an obvious amorphous structure when the Na_2WO_4 concentration was 5~15 g/L, while Ni-W-P coatings changed from amorphous structure to microcrystalline structure when the Na_2WO_4 concentration exceeded 15 g/L. The surface morphologies of Ni-W-P coatings which were relatively flat and dense without defects, such as cracks and holes showed cellular structure, especially when the concentration of Na_2WO_4 is 15 g/L.

(2) The effects of different concentrations of Na_2WO_4 on deposition rate, phase composition, and corrosion resistance of Ni-W-P coatings were analyzed. When the concentration of Na_2WO_4 in the plating solution was 15 g/L, the deposition rate of Ni-W-P coating was the fastest, about 17 um/h, the corrosion rate was the slowest, about 0.0903 $g/m^2 \cdot h$, the maximum self-corrosion potential was -0.326 V, the minimum corrosion current was 0.003 A/cm^2, and the capacitance arc radius was the largest. Therefore, Ni-W-P coating with 15 g/L Na_2WO_4 can significantly improve the corrosion resistance of magnesium alloy substrate.

(3) The adhesion between Ni-W-P coating and magnesium alloy substrate and micro-hardness of Ni-W-P coatings were gradually improved with an increasing of Na_2WO_4 concentration in the plating solution. When Na_2WO_4 was added at 20 g/L, Ni-W-P coating had the best bond with magnesium alloy substrate and the maximum Vickers micro-hardness of Ni-W-P coatings is 348.3 Hv.

5. Acknowledgments

The work was supported by the National Natural Science Foundation of China (50172023) and the Shaanxi Industrial Science and Technology Research (2014K08-09) and the Key Research and Development Program of Shaanxi Province of China (2020GY-115).

6. References

1. Duan M, Luo L, Liu Y. Microstructural evolution of AZ31 Mg alloy with surface mechanical attrition treatment: grain and texture gradient. J Alloys Compd. 2020;823:153691.
2. Song JF, She J, Chen DL, Pan FS. Latest research advances on magnesium and magnesium alloys worldwide. J. Magnesium Alloys. 2020;8(1):1-41.
3. Abdi-Alghanab K, Seifzadeh D, Rajabalizadeh Z, Habibi-Yangjeh A. High corrosion protection performance of the LDH/Ni-P composite coating on AM60B magnesium alloy. Surf Coat Tech. 2020;397:125979.
4. Ribeiro EP, Couto AA, Oliveira LA, Antunes RA. Influence of the treatment time on the surface chemistry and corrosion behavior of cerium-based conversion coatings on the AZ91D magnesium alloy. Mater Res Iberoam J Mater. 2019;22(Suppl. 1).
5. Selvi VE, Chatterji P, Subramanian S, Balaraju JN. Autocatalytic duplex Ni-P/Ni-W-P coatings on AZ31B magnesium alloy. Surf Coat Tech. 2014;240:103-9.

6. Shoghi P, Seifzadeh D, Gholizadeh-Gheshlaghi M, Habibi-Yangjeh A. Pretreatment-free Ni-P plating on magnesium alloy at low temperatures. Trans Nonferrous Met Soc China. 2018;28(12):2478-88.
7. Luo H, Leitch M, Zeng HB, Luo JL. Characterization of microstructure and properties of electroless duplex Ni-W-P/Ni-P nano-ZrO_2 composite coating. Mater Today Phys. 2018;4:36-42.
8. Chen S, Wan P, Zhang B, Eren Erişen D, Yang H, Yang K. A novel polymer critical re-melting treatment for improving corrosion resistance of magnesium alloy stent. J Mater Sci Technol. 2019;35(1):19-22.
9. Tasci S, Ozden RC, Anik M. Corrosion and wear characteristics of electroless Ni-P, Ni-P-W and composite Ni-P-W/Al_2O_3 coatings on AZ91 sheet. Met Mater Int. 2019;25(2):313-23.
10. Xiu-qing X, Jian M, Zhen-quan B, Yao-rong F, Qiu-rong M, Wen-zhen Z. The corrosion behavior of electroless Ni–P coating in Cl^-/H_2S environment. Appl Surf Sci. 2012;258(22):8802-6.
11. Liu H, Lv YY, Liu Z, Liu H, Thompson GE. Dry sliding wear behaviour and structural characteristics of laser-annealed electroless Ni-P/Ni-Mo-P duplex coatings. Tribol Int. 2016;103:343-51.
12. Zhang YG, Sun WC, Ma M, Tian SS, Liu YW, Xiao Y. Effect of MoS_2 concentration on microstructure and tribological behavior of electrophoretic-electrodeposited Ni-Co-Al_2O_3-MoS_2 composites. Mater Res. 2020;23(5):e20200296.
13. Ma M, Sun WC, Zhang YG, Liu YW, Dong YR, Zi JY, et al. Effect of TiC particles concentration on microstructure and properties of Ni-TiC composite coatings. Mater Res. 2019;22(6):e20190530.
14. Chen C-A, Jian S-Y, Lu C-H, Lee C-Y, Aktuğ SL, Ger M-D. Evaluation of microstructural effects on corrosion behavior of AZ31B magnesium alloy with a MAO coating and electroless Ni-P plating. J Mater Res Technol. 2020;9(6):13902-13.
15. Huang ZH, Zhou YJ, Nguyen TT. Study of nickel matrix composite coatings deposited from electroless plating bath loaded with TiB_2, ZrB_2 and TiC particles for improved wear and corrosion resistance. Surf Coat Tech. 2019;364:323-9.
16. Zuleta AA, Correa E, Castano JG, Echeverria F, Baron-Wiechec A, Skeldon P, et al. Study of the formation of alkaline electroless Ni-P coating on magnesium and AZ31B magnesium alloy. Surf Coat Tech. 2017;321:309-20.
17. Sezer N, Evis Z, Kayhan SM, Tahmasebifar A, Koc M. Review of magnesium-based biomaterials and their applications. J Magnesium Alloys. 2018;6(1):23-43.
18. Yu WB, Chen DQ, Tian L, Zhao HB, Wang XJ. Self-lubricate and anisotropic wear behavior of AZ91D magnesium alloy reinforced with ternary Ti2AlC MAX phases. J Mater Sci Technol. 2019;35(3):275-84.
19. Oliveira MCL, Correa OV, Ett B, Sayeg IJ, de Lima NB, Antunes RA. Influence of the tungsten content on surface properties of electroless Ni-W-P coatings. Mater Res Iberoam J Mater. 2018;21(1):20.
20. Singh C, Tiwari SK, Singh R. Deposition and characterization of electroless Ni on fluoride free pretreated AZ91 magnesium alloy. Mater Today Proc. 2018;5:17312-9.
21. Rajabalizadeh Z, Seifzadeh D. Application of electroless Ni-P coating on magnesium alloy via CrO_3/HF free titanate pretreatment. Appl Surf Sci. 2017;422:696-709.
22. Rajabalizadeh Z, Seifzadeh D, Habibi-Yangjeh A, Mesri Gundoshmian T, Nezamdoust S. MesriGundoshmian T, Nezamdoust S. Electrochemical noise analysis to examine the corrosion behavior of Ni-P deposit on AM60B alloy plated by Zr pretreatment. Surf Coat Tech. 2018;346:29-39.
23. Chen X, Li G, Lian J. Deposition of electroless Ni-P/Ni-W-P duplex coatings on AZ91D magnesium alloy. Trans Nonferrous Met Soc China. 2008;18(z1):323-8.
24. Guo HJ, Fan JF, Zhang H, Zhang Q, Wu YC, Li WG, et al. The preparation and mechanical properties of nano-magnesium alloy bulks. J Alloys Compd. 2020;819:153253.
25. Sun L, Ma Y, Wang JS, An LY, Wang S, Wang ZY. Preparation and corrosion resistance of hybrid coatings formed by PEN/C plus PEO on AZ91D magnesium alloys. Surf Coat Tech. 2020;390:125661.
26. Zhou P, Cai WB, Yang YB, Li XJ, Zhang T, Wang FH. Effect of ultrasonic agitation during the activation process on the microstructure and corrosion resistance of electroless Ni-W-P coatings on AZ91D magnesium alloy. Surf Coat Tech. 2019;374:103-15.
27. Forero López AD, Lehr IL, Brugnoni LI, Saidman SB. Improvement in the corrosion protection and bactericidal properties of AZ91D magnesium alloy coated with a microstructured polypyrrole film. J Magnesium Alloys. 2018;6(1):15-22.
28. Armyanov S, Valova E, Tatchev D, Georgieva J. Electroless deposited ternary alloys: third element chemical state, localisation and influence on the properties: a short review. Trans Inst Met Finish. 2018;96(1):12-9.
29. Bahramian A, Eyraud M, Vacandio F, Knauth P. Improving the corrosion properties of amorphous Ni-P thin films using different additives. Surf Coat Tech. 2018;345:40-52.
30. Yang HJ, Gao YM, Qin WC, Li YF. Microstructure and corrosion behavior of electroless Ni-P on sprayed Al-Ce coating of 3003 aluminum alloy. Surf Coat Tech. 2015;281:176-83.
31. Shao QQ, Zhang X, Cui ZJ, Tan XF. Study on corrosion resistance of Ni-W-P coating in hypersaline brine. Acta Geol Sin. 2014;88:387-8.
32. Shu X, He Z, Wang YX, Yin L. Mechanical properties of Ni-based coatings fabricated by electroless plating method. Surf Eng. 2020;36(9):944-51.
33. Biswas A, Das SK, Sahoo P. Investigation of the tribological behavior of electroless Ni-W-P coating pre and post phase transformation regime. Mater Res Express. 2019;6(9):0965c1.
34. Dong YR, Sun WC, Liu XJ, Jia JW, Guo F, Ma M, et al. Effect of CNTs concentration on the microstructure and friction behavior of Ni-GO-CNTs composite coatings. Surf Coat Tech. 2019;359:141-9.
35. Seifzadeh D, Kazemi Mohsenabadi H, Rajabalizadeh Z. Electroless Ni-P plating on magnesium alloy by innovative, simple and non-toxic oxalate pretreatment and its corrosion protection. RSC Advances. 2016;6(99):97241-52.
36. Lian JS, Li GY, Niu LY, Gu CD, Jiang ZH, Jiang Q. Electroless Ni-P deposition plus zinc phosphate coating on AZ91D magnesium alloy. Surf Coat Tech. 2006;200(20-21):5956-62.